



**AFRL-RX-WP-TR-2010-4185**

**COLLABORATIVE RESEARCH AND DEVELOPMENT  
(CR&D)**

**Task Order 0035: Incorporation of Metal Nanoshells into Photovoltaic  
Devices**

**Joseph R. Cole and Naomi J. Halas**

**Rice University**

**JULY 2007**

**Final Report**

**Approved for public release; distribution unlimited.**

*See additional restrictions described on inside pages*

**STINFO COPY**

**AIR FORCE RESEARCH LABORATORY  
MATERIALS AND MANUFACTURING DIRECTORATE  
WRIGHT-PATTERSON AIR FORCE BASE, OH 45433-7750  
AIR FORCE MATERIEL COMMAND  
UNITED STATES AIR FORCE**

## NOTICE AND SIGNATURE PAGE

Using Government drawings, specifications, or other data included in this document for any purpose other than Government procurement does not in any way obligate the U.S. Government. The fact that the Government formulated or supplied the drawings, specifications, or other data does not license the holder or any other person or corporation; or convey any rights or permission to manufacture, use, or sell any patented invention that may relate to them.

This report was cleared for public release by the USAF 88<sup>th</sup> Air Base Wing (88 ABW) Public Affairs Office (PAO) and is available to the general public, including foreign nationals. Copies may be obtained from the Defense Technical Information Center (DTIC) (<http://www.dtic.mil>).

AFRL-RX-WP-TR-2010-4185 HAS BEEN REVIEWED AND IS APPROVED FOR PUBLICATION IN ACCORDANCE WITH THE ASSIGNED DISTRIBUTION STATEMENT.

\*//Signature//

---

MARK GROFF  
Program Manager  
Business Operations Branch  
Materials & Manufacturing Directorate

//Signature//

---

KENNETH A. FEESER  
Branch Chief  
Business Operations Branch  
Materials & Manufacturing Directorate

This report is published in the interest of scientific and technical information exchange, and its publication does not constitute the Government's approval or disapproval of its ideas or findings.

\*Disseminated copies will show “//Signature//” stamped or typed above the signature blocks.

<b>REPORT DOCUMENTATION PAGE</b>				<i>Form Approved</i> OMB No. 0704-0188	
The public reporting burden for this collection of information is estimated to average 1 hour per response, including the time for reviewing instructions, searching existing data sources, gathering and maintaining the data needed, and completing and reviewing the collection of information. Send comments regarding this burden estimate or any other aspect of this collection of information, including suggestions for reducing this burden, to Department of Defense, Washington Headquarters Services, Directorate for Information Operations and Reports (0704-0188), 1215 Jefferson Davis Highway, Suite 1204, Arlington, VA 22202-4302. Respondents should be aware that notwithstanding any other provision of law, no person shall be subject to any penalty for failing to comply with a collection of information if it does not display a currently valid OMB control number. <b>PLEASE DO NOT RETURN YOUR FORM TO THE ABOVE ADDRESS.</b>					
<b>1. REPORT DATE (DD-MM-YY)</b> July 2007		<b>2. REPORT TYPE</b> Final		<b>3. DATES COVERED (From - To)</b> 08 June 2005 – 07 June 2007	
<b>4. TITLE AND SUBTITLE</b> COLLABORATIVE RESEARCH AND DEVELOPMENT (CR&D) Task Order 0035: Incorporation of Metal Nanoshells into Photovoltaic Devices				<b>5a. CONTRACT NUMBER</b> F33615-03-D-5801-0061	
				<b>5b. GRANT NUMBER</b>	
				<b>5c. PROGRAM ELEMENT NUMBER</b> 62102F	
<b>6. AUTHOR(S)</b> Joseph R. Cole and Naomi J. Halas				<b>5d. PROJECT NUMBER</b> 4349	
				<b>5e. TASK NUMBER</b> L0	
				<b>5f. WORK UNIT NUMBER</b> 4349L0VT	
<b>7. PERFORMING ORGANIZATION NAME(S) AND ADDRESS(ES)</b> Rice University Houston, TX				<b>8. PERFORMING ORGANIZATION REPORT NUMBER</b> S-531-035	
<b>9. SPONSORING/MONITORING AGENCY NAME(S) AND ADDRESS(ES)</b> Air Force Research Laboratory Materials and Manufacturing Directorate Wright-Patterson Air Force Base, OH 45433-7750 Air Force Materiel Command United States Air Force				<b>10. SPONSORING/MONITORING AGENCY ACRONYM(S)</b> AFRL/RXOB	
				<b>11. SPONSORING/MONITORING AGENCY REPORT NUMBER(S)</b> AFRL-RX-WP-TR-2010-4185	
<b>12. DISTRIBUTION/AVAILABILITY STATEMENT</b> Approved for public release; distribution unlimited.					
<b>13. SUPPLEMENTARY NOTES</b> PAO Case Number: 88ABW 2010-1227; Clearance Date: 17 Mar 2010. Report contains color.					
<b>14. ABSTRACT</b> This research in support of the Air Force Research Laboratory Materials and Manufacturing Directorate was conducted at Wright-Patterson AFB, Ohio from 8 June 2005 through 7 June 2007. The plasmon resonance in metallic nanoshells can be used to efficiently harvest solar energy and convert it into thermal or electronic form. Possible applications include improved optical coupling into silicon photodiodes, solar water heaters, and photocatalysis. We use standard optimization algorithms to theoretically determine the best mixture of different nanoshell species ([core, shell] sizes) for two practical scenarios. We show that a mixture of nanoshell species $[r_1, r_2] = [47, 58]$ nm and $[r_1, r_2] = [28, 42]$ nm in a 6:5 volume ratio is optimal for absorbing AM 1.5 sunlight when deposited on a silicon surface. Surprisingly, we find that a single particle species is very good for scattering AM 1.5 light on a glass surface, and that very little benefit is gained by mixing different shells. Assumptions and approximations made in the analysis are discussed.					
<b>15. SUBJECT TERMS</b> metal nanoshells, solar applications					
<b>16. SECURITY CLASSIFICATION OF:</b>			<b>17. LIMITATION OF ABSTRACT:</b> SAR	<b>18. NUMBER OF PAGES</b> 60	<b>19a. NAME OF RESPONSIBLE PERSON (Monitor)</b> Mark Groff  <b>19b. TELEPHONE NUMBER (Include Area Code)</b> N/A
<b>a. REPORT</b> Unclassified	<b>b. ABSTRACT</b> Unclassified	<b>c. THIS PAGE</b> Unclassified			

# Contents

List of Figures	iv
Preface	v
Acknowledgements	vii
<b>Chapter 1 – Plasmonic Particles, Sunlight, and Optimization</b>	<b>1</b>
Nanoshell Physics	1
The Solar Spectrum	9
Numerical Optimization	12
<b>Chapter 2 – Description of the Algorithm</b>	<b>16</b>
Overview of the Code	16
Use of the Code	18
Inherent Approximations	21
<b>Chapter 3 – Two Scenarios in Detail</b>	<b>27</b>
Absorption of Sunlight on a Silicon Photodiode	27
Scattering of Sunlight from a Glass Surface	30
<b>Chapter 4 – Conclusions and Future Work</b>	<b>34</b>
Appendix A – Code	35
solar_fit.m	35
find_local_min.m	37
residual.m	38
next_combo.m	39
load_spec_am1_5.m	40
load_shell_data.m	41
pick_lambdas.m	42
Appendix B – Surface Coverage Calculation	43
Appendix C – Number of Interparticle Couplings on a Surface	44
References	45

## List of Figures

Figure 1.1 – Geometry of a nanoshell	5
Figure 1.2 – Hybridization of sphere and cavity plasmon modes	6
Figure 1.3 – Nanoshell tunability	7
Figure 1.4 – Poynting vector diagram	8
Figure 1.5 – Standard solar spectra, with 5800 K blackbody overlay	10
Figure 1.6 – Diagram of air mass geometry	11
Figure 1.7 – Golden section search and parabolic interpolation	12
Figure 1.8 – Simplex method	14
Figure 2.1 – Variation of minimization function with coverage	20
Figure 2.2 – Dielectric environment of a nanoshell	23
Figure 2.3 – Coupled versus independent scatterers	24
Figure 2.4 – Angular dependence of scattering	25
Figure 3.1 – Optimal absorption on silicon, 40% coverage	28
Figure 3.2 – Optimal absorption on silicon, 50% coverage	29
Figure 3.3 – Absorption of soot	30
Figure 3.4 – Optimal scattering from glass	31
Figure 3.5 – Scattering from $\text{TiO}_2$	32
Figure B.1 – Hexagonal array of nanoparticles	43

## Preface

If a television commercial by General Electric, which aired in May 2003, about a nanotechnologist and supermodel who fall in love at first sight were to be taken as evidence, we could conclude that nanotechnology has replaced rocket science as the discipline of the ultra-chic über-geek. Movies such as Spiderman and Minority Report, and mass market literature like Prey have shaped public consciousness of the term so that it elicits images of tiny miracle working robots and lethal gray goo. In fact, Merriam-Webster's Online Dictionary gives this definition: "the art of manipulating materials on an atomic or molecular scale especially to build microscopic devices (as robots)." But most serious research in the field of nanotechnology is not about trying to build tiny robots, and there are plenty of less glamorous disciplines like chemistry or materials science that are focused on manipulating materials on an atomic or molecular scale. So, what separates nanotechnology from other buzzwords like "lockbox" or "smoking gun" which are just plagiarisms of emotionally charged language with little substance?

For me, nanotechnology is meaningful and different from other scientific disciplines because it is about *engineering* solutions to problems that take advantage of the unique, controllable properties of nanoscale matter. When the characteristic length scale of an object is a billionth of a meter, quantum mechanics allows for physical properties that do not exist in the macroscopic world. For the first time in history, we can change some parameter of a simple nanoscale system, which alters some system property in a well understood way, so that we can achieve some a priori design goal.

Nanotechnology is a notoriously difficult word to define, and I am certain that my

definition is little better than Merriam-Webster's, but this is how I differentiate the field from others.

This thesis is about how a particular nanoscale particle, the nanoshell, can be used in a system to achieve optimal energy conversion from electromagnetic form to thermal or electronic form. I wrote computer code that calculates the optimal mixture of nanoshell geometries, or species, for absorbing or scattering a given spectrum of light. The code is intended to be sufficiently general so that it will be a useful design tool for a wide variety of engineering problems, but I solved only two very specific scenarios which are of interest to our work in the Laboratory for Nanophotonics at Rice University. I hope this work will be valuable in the design and construction of novel devices with practical use, and I hope it will stand as a realistic example of the current state of nanotechnology and its near-term potential.

## Acknowledgments

I am deeply indebted to many individuals without whom I absolutely could not have completed this work. I would like to thank all of the Halas group members, past and present, for lively discussions, late night company, sympathy, empathy, and motivational support during what can often be a grind-you-up-and-spit-you-out process that is much easier to walk away from than endure. In particular, I owe Felicia Tam, Nate Grady, and Surbhi Lal more than a few beers for reading what might be described as a “*very rough*” draft of this work. Also, I am deeply grateful to my advisor, Naomi Halas, and all my committee members for constructive criticism of my work. They made every possible effort to mold me into something resembling a scientist and generally endeavored to keep my head on straight. Finally, thanks are owed to all my friends and family; these are the people who made me what I am today, and any quality I possess is brought out by their influence. Above all, I owe everything to my wife Elizabeth, whose unwavering support, impeccable work ethic, and undying confidence in my capabilities gave me the momentum I needed to see this process through. She inspires me and completes me, and I am a better person simply for having met her.

## **Chapter 1 – Plasmonic Particles, Sunlight, and Optimization**

The Sun is the energy source of life, and nature stockpiled that energy into convenient forms like coal and oil over the course of millennia. We are entering an age when depletion of these reserves causes us to question the long term sustainability of life as we know it. It is critical that we develop sustainable processes for the production of food, potable water, and the extraction of resources required for manufacturing and construction. Success in these goals hinges on our ability to generate renewable energy. Energy from the Sun is abundant, clean, and most importantly, sustainable, but we lack methods to harness it efficiently. New discoveries in nanotechnology hold great promise toward that end<sup>1, 2, 3</sup>. In this work, I examine theoretically how one nanoscale technology, the nanoshell, can be used to optimally absorb or scatter the energy in sunlight, which would allow us to convert it into usable electronic or thermal form.

### **Nanoshell Physics**

The photophysics of nanoshells is intimately related to the plasmon resonance of the particles. Plasmons are collective oscillations of the conduction electrons in a metal, and they can dominate the metal's optical properties when certain conditions are met. This strong interaction between light and matter enables efficient coupling of electromagnetic energy into the metal, and the strength of the interaction is determined by the geometry of the object as well as its dielectric function. The dielectric function describes how an electric field causes a polarization response<sup>4</sup> in a given material. It is a measure of how charged particles like electrons respond to light, so it depends on the

density of free electrons present and the electron mean free path. Generally, the dielectric function is complex-valued, and it varies with the frequency of the applied electric field.

The origin of plasmons is most easily understood in terms of Drude's simple classical description of conductivity in metal<sup>5</sup>. Drude applied a kinetic theory usually associated with the description of an ideal gas to explain macroscopic phenomena in metals. He assumed that electrons could be treated as a gas that is essentially free, but that is confined by the boundaries of the metal. The electrons are independent in that they do not interact with one another, but they do scatter off of the positive ion cores of the crystal lattice. Drude's model explains AC and DC conductivity in metals, the Hall effect, and thermal conductivity surprisingly well considering the crude approximations he used.

The model predicts a zero in the dielectric function at a certain frequency,

$$\omega_B = \sqrt{\frac{4\pi n e^2}{m}},$$

known as the bulk plasma frequency, where  $n$  is the electron density,  $e$  is the electronic charge, and  $m$  is the electron mass, all in CGS units. This frequency marks the boundary between solutions to the wave equation that can propagate ( $\omega > \omega_B$ , the material is transparent), and those that cannot ( $\omega < \omega_B$ , the field decays exponentially)<sup>5</sup>.

Furthermore, when  $\omega = \omega_B$ , a solution to a different wave equation, for charge density waves, exists. At that exact frequency, collective oscillations of free electrons, or plasmons, are possible.

More precisely,  $\omega = \omega_B$  is the condition that must be met for the electron charge density to have oscillatory time dependence. The oscillations arise because collective

displacement of electrons in one direction will uncover the fixed positive ion cores of the crystal lattice. These cores provide a restoring force on the displaced electron “gas” through Coulombic attraction, and a harmonic oscillation results. The alkali metals are particularly well described by the Drude model<sup>5</sup>. The noble metals are as well, but to a lesser extent because interband transitions from the d- to sp-orbital in the atomic lattice dominate the electronic response at short visible wavelengths<sup>6</sup>. Other materials require quantum mechanical models to explain their observed dielectric functions.

Since plasmons originate from the Drude response of a material, they are only observable in metals that have dielectric functions dominated by the Drude term. However, bulk plasmons have never been directly observed in practice, even for alkali or noble metals, although they undoubtedly exist. Bulk plasmons are so difficult to observe because they cannot be directly excited by light. At optical frequencies, bulk metals have a skin depth on the order of a few tens of nanometers<sup>6</sup>. Electrons on the interior of the bulk are left undisturbed because of the screening effect of the surface electrons. The most direct evidence available for the existence of bulk plasmons is the observation of energy losses in multiples of  $\hbar\omega_B$  when electrons are fired through thin metallic films<sup>7</sup>.

As mentioned above, geometry also plays a significant role in the interaction of light with matter. The easiest way to understand the influence of shape is through Maxwell’s electromagnetic theory. Maxwell’s equations tell us that the tangential component of a magnetic field and the normal component of the electric flux density will be discontinuous at a boundary between two dissimilar dielectric media<sup>8</sup>. These boundary conditions give rise to the importance of geometry in the solutions of wave equations and therefore the optical properties of materials. In the simplest case,

Maxwell's equations predict the existence of charge density waves with a frequency of  $\frac{\omega_B}{\sqrt{2}}$  along a surface at the boundary of an infinite conductor in contact with a dielectric medium. These waves are known as surface plasmons.

Unlike bulk plasmons, surface plasmons can be excited by light, but alas, not directly. They require the presence of an optical coupler that can add enough momentum to what is already present in light to excite traveling wave plasmons. Examples of optical couplers include prisms or gratings. More information about how these add to the momentum of light so that surface plasmons can be excited is available in Surface Plasmons on Smooth and Rough Surfaces by Raether<sup>9</sup>.

Fortunately, when a particle is very small, comparable to the wavelength of light, standing wave solutions to the surface charge density wave equation appear. These local charge density fluctuations can be directly excited by light and are the phenomena I refer to when I use the word "plasmon" hereinafter. The fact that plasma oscillations in macroscopic media are so difficult to excite is primarily responsible for the late arrival of technology to exploit them. The advent of nanoscale control of metallic particle geometries enables scientists and engineers to use plasmons in a wide range of applications from medicine<sup>10</sup>, to sensor technologies<sup>11</sup>, to light harvesting and energy conversion<sup>12</sup>.

Nanoshells are particularly interesting plasmonic particles because their plasmon resonance is controllably tunable over the entire visible light spectrum as well as the near to mid-infrared domain. Nanoshells are spherical core-shell particles typically made using silica cores coated with thin gold or silver shells. In Figure 1.1,  $r_1$  is the radius of the inner core, and  $r_2$  is the overall radius of the particle. Their optical properties stem

from the interaction, or hybridization, between the plasmon resonances of two elementary geometries, that of a nanoscale conducting sphere in an infinite dielectric medium and of a nanoscale dielectric cavity in an infinite conducting medium.

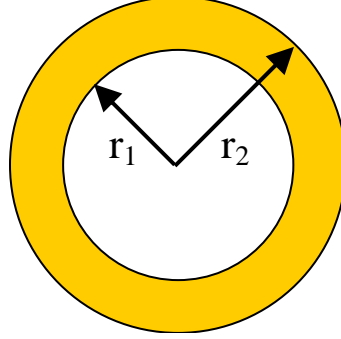


Figure 1.1 The geometry of a nanoshell

Mie solved Maxwell's equations for spherical geometries in 1908<sup>13</sup>. The theory was extended by Aden and Kerker for radially symmetric core-shell geometries in 1951<sup>14</sup>. Mie theory predicts that a conducting sphere will have plasmon resonances at  $\omega_B \sqrt{\frac{l}{2l+1}}$ , where  $l$  is a positive integer quantum number. Similarly, it predicts plasmon resonances at  $\omega_B \sqrt{\frac{l+1}{2l+1}}$  for a cavity. The  $l = 1$  mode is known as the dipole resonance,  $l = 2$  is the quadrupole, and so on. In a nanoshell geometry, the elementary sphere and cavity modes hybridize in rigorous analogy with molecular orbital theory<sup>15</sup>. Plasmon hybridization theory is the best way to gain an intuitive understanding of how to engineer the optical behavior of nanoshells. Coulombic forces mediate the interaction between the modes, so that the thickness of the metallic shell layer controls the strength of the hybridization.

Hybridization between sphere and cavity dipole modes is shown in Figure 1.2. The cavity mode has energy equal to  $\sqrt{\frac{2}{3}}\omega_B$ , 1.41 times higher than the energy of the

sphere plasmon at  $\sqrt{\frac{1}{3}}\omega_B$ . In the thick shell limit, the “bonding” and “antibonding” hybridized modes are only weakly coupled, so they are nearly equal in energy to their constituent parts. The antibonding mode is known as the dark plasmon because it has no net dipole moment and cannot normally be excited by light, while the bonding mode is called the bright plasmon. As the shell becomes thinner, the Coulombic force increases, and the dark plasmon blue-shifts in energy, while the bright plasmon red-shifts.

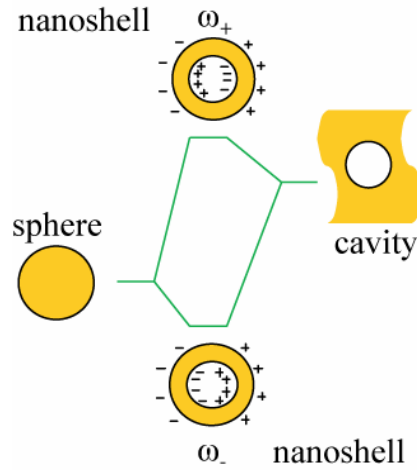


Figure 1.2 Hybridization of sphere and cavity plasmon modes to make the nanoshell plasmon

In addition to plasmon hybridization theory, resonance energy is affected by overall particle size. Just as the pitch of a large ringing bell is lower (longer wavelength) than smaller bells, the standing wave resonance of large nanoparticles occurs at longer wavelengths. The combination of this effect with plasmon hybridization enables the unique tunability of nanoshells.

Since plasmons are excitable by light directly, their existence can be experimentally verified by measuring light extinction in a spectrophotometer. Extinction is the amount of light scattered or absorbed by the particle. At wavelengths near the

resonance energy, light interacts very strongly with the particle, and the extinction spectrum will show a pronounced peak. Spectra measured in this way are well-fit by extinction efficiency spectra calculated using Mie theory<sup>16</sup>. Efficiency is the ratio of the particle's effective cross section to its geometrical cross section. Figure 1.3 shows how spectra calculated using Mie theory can be explained in terms of the plasmon hybridization model.

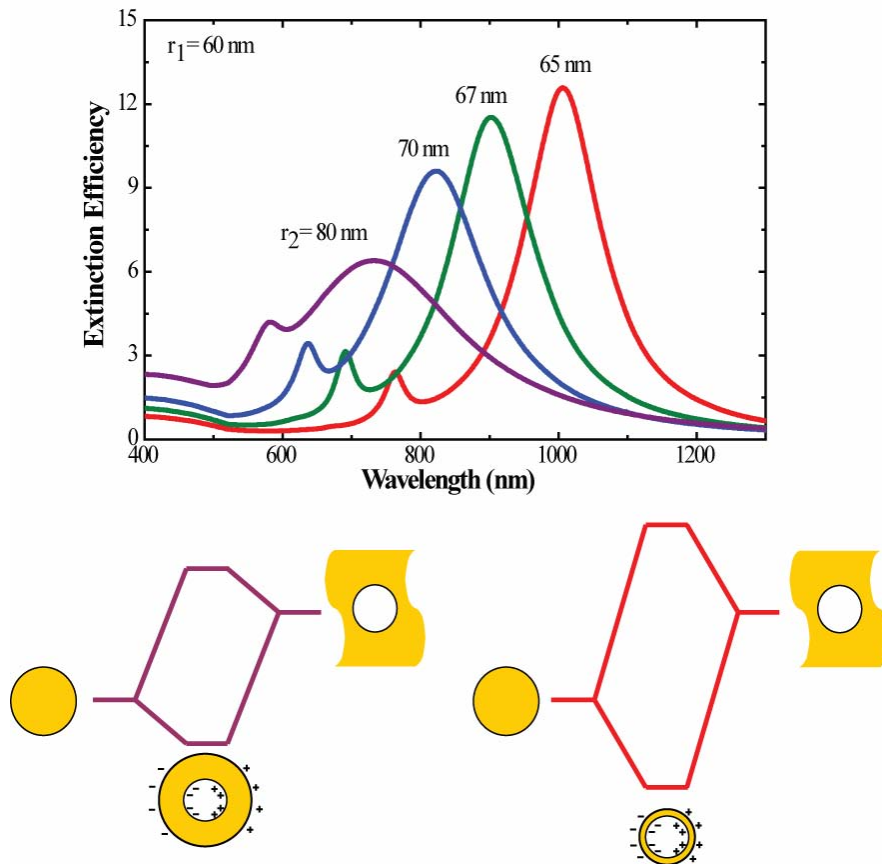


Figure 1.3 Hybridization controls plasmon resonance wavelength  
 On the left, thicker shells result in less interaction  
 On the right, thinner shells result in more interaction

The extinction efficiency of plasmonic particles can range from several times greater than one when on-resonance to less than one. From a geometrical optics standpoint, it does not make sense for any object to have an effective cross section larger

than its area projected onto the plane of incidence. However, geometrical optics breaks down for nanoscale objects. Ultimately, light is just a wave of time-varying electric and magnetic fields, and an object in the light's path interacts with all the nearby fields, not just those directly incident upon it. Consider Figure 1.4, the Poynting vector diagram for a small metallic particle near its plasmon resonance. The Poynting vector is found by taking the cross product of the electric and magnetic field vectors, and it represents the flow of energy in the system. The particle seems to pull the light toward it from all directions<sup>17, 18</sup>. For off-resonance particles, the opposite is observed. The effective cross section is really a simplification of the complicated way light interacts with nearby matter.

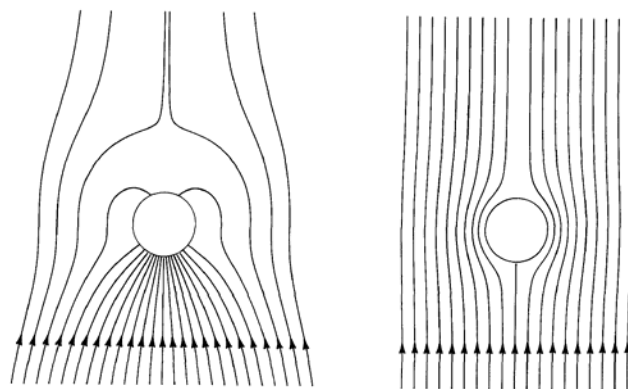


Figure 1.4 Poynting vector diagram of a plasmonic particle on-resonance (left) and off-resonance (right) (Reprinted with permission. Copyright 1983, American Association of Physics Teachers<sup>17</sup>)

So, plasmon hybridization and particle size explain the position of the resonance peaks shown in a plot of extinction efficiency, and consideration of energy flow around the particle can explain the peak height. Only the breadth of the peak remains to be explained. Two factors influence peak width. The first is the plasmon dephasing time, or the length of time a collective oscillation of electrons can exist before it disappears as a result of frictional damping against scattering centers. Plasmon dephasing is a

manifestation of the fact that perfect single-frequency signals are impossible in real life; such a signal would have to last an infinitely long time. Since the plasmon has a finite lifetime, taking the Fourier transform will result in a peak that is not perfectly sharp, where the peak width is an indication of the plasmon dephasing time. Second, in ensemble measurements plasmon line width is a result of polydispersity in the nanoshell suspension. There will always be some distribution of core size and shell thickness. Typically, cores might be  $\pm 5\%$  from the mean size and shells might be  $\pm 1\%$ . An ensemble measurement of the light extinction for such a group of particles will show an average of the many slightly varied plasmon resonances.

### **The Solar Spectrum**

In space, our Sun has the emission spectrum one would expect from a 5800 K blackbody<sup>19, 20</sup>. However, the light that reaches the surface of the Earth is scattered and refracted by the atmosphere, so its path from space to the ground plays a crucial role in the spectrum an observer sees. Since the spectrum on the ground can vary greatly, the American Society for Testing and Materials (ASTM) developed the ASTM G-173-03 standard solar spectra. The spectral data can be downloaded for free from the National Renewable Energy Laboratory's (NREL) website<sup>21</sup>. Figure 1.5 shows the spectra with the blackbody curve overlaid. Manufacturers of photovoltaic devices and other solar energy technologies report performance in terms of these spectra in order to facilitate meaningful comparisons between technologies or products. Usually, the AM 1.5 spectrum is used because it represents time-averaged irradiation over one day.

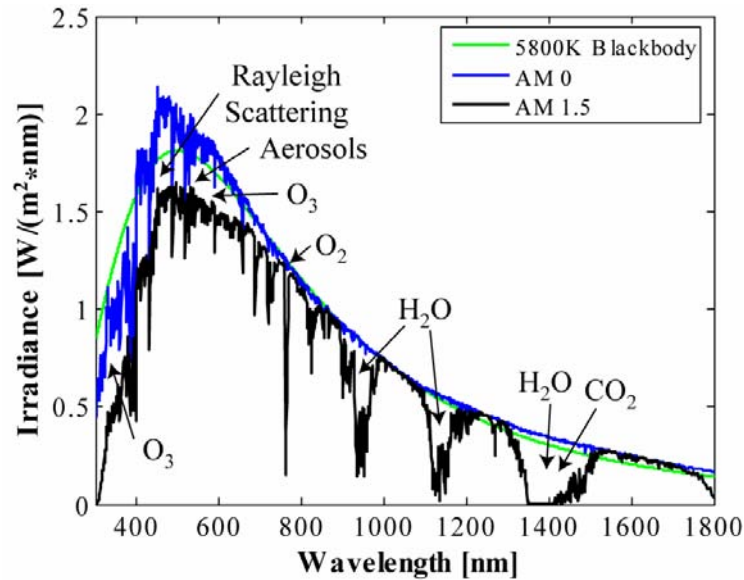


Figure 1.5 Standard solar spectra, with 5800 K blackbody overlay

Three spectra are included in the standard: AM 0, total global AM 1.5, and direct normal AM 1.5. “AM” stands for air mass, and it is a measure of the amount of atmosphere light must travel through before reaching the surface. AM 0 refers to the spectrum incident on Earth in outer space before passing through any atmosphere. AM 1 is the spectrum on the ground at high noon, when the sun is at its zenith. As the time of day continues past noon, the Sun will rotate away from zenith, and the atmospheric path length of its light increases. When the path length is equal to 1.5 times the length at zenith, an observer would see the AM 1.5 spectrum. This occurs when the sun is  $48.2^\circ$  past zenith, as can be seen from Figure 1.6. In the figure, the curved atmosphere is approximated by a line tangent to the outer atmosphere and normal to the AM 1 path, forming a right triangle. As long as the angle from zenith is  $\leq 60^\circ$ , the approximation is valid. The difference between the total global and the direct normal spectra is that the direct normal spectrum only includes light that arrives directly from the Sun. Light that

would be incident elsewhere, but is scattered toward the observer is not included. The total global spectrum includes all contributions, and it is the spectrum used for this work.

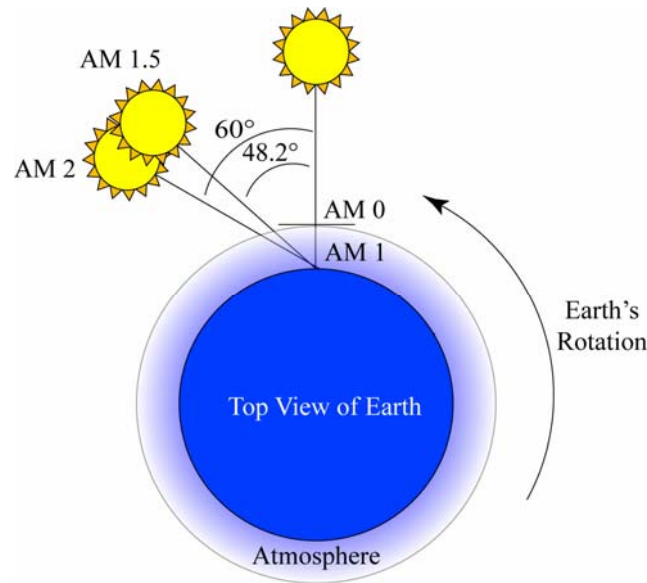


Figure 1.6 Diagram of air mass geometry

The AM 1.5 standard spectrum includes all of the major effects of scattering and absorption that occur as light passes through the Earth's atmosphere. It is calculated for a plane with surface normal directed at the Sun and tilted toward the equator at  $37^\circ$ , chosen because it represents an average latitude for the 48 contiguous United States. It is calculated based on a standard atmosphere for the United States with average temperature, pressure, aerosol density, air density, and molecular species density. Also included are estimates of turbidity, water vapor content, ozone content, and surface spectral albedo (reflectivity of the soil). The contributions of some of these effects are labeled in Figure 1.5.

## Numerical Optimization<sup>22</sup>

Optimization is the problem of finding a global maximum or minimum of a given function. These two processes are equivalent because maximizing a function  $f(x)$  is the same as minimizing  $-f(x)$ . There are many well-known optimization algorithms, but I use only two that are relatively straightforward for the present work. One, called Brent's method<sup>23</sup>, is useful for solving one-dimensional optimization problems. The other is known as the simplex method<sup>24</sup> because it solves multi-dimensional problems by manipulation of a geometrical structure called a simplex along the topology of the function. Both these methods are straightforward in that they do not require the derivative of the function to be calculated. Furthermore, they are easily implemented in code; in fact, Mathworks includes them as built-in functions in Matlab.

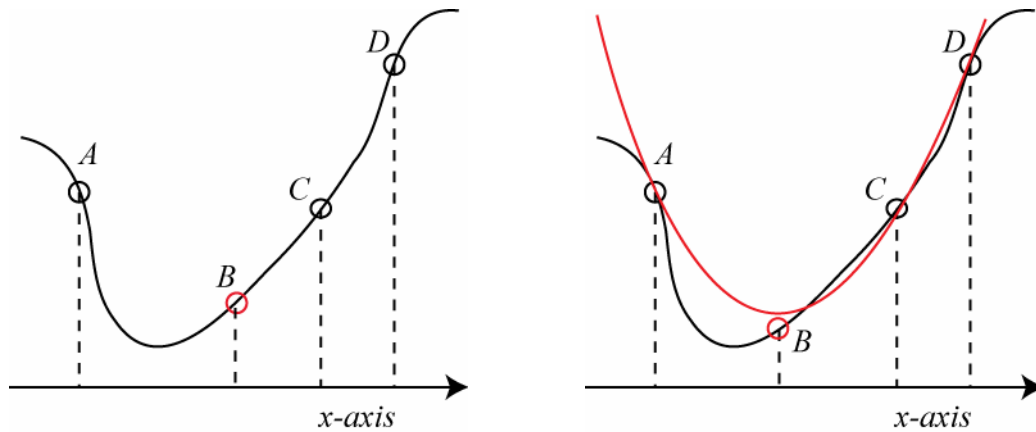


Figure 1.7 Graphical representation of the golden section search (left) and parabolic interpolation (right). A and D bracket the search interval, C is the current known minimum. The next iteration will try point B. Since B is less than C, B will replace C and C will replace D; if B were greater than C, B would replace A.

Brent's method uses a combination of the golden section search and parabolic interpolation to quickly and robustly find a minimum with the fewest possible number of function evaluations. The method requires that the minimum be bracketed between two

points. Golden section search is a slow but sure way to converge on the minimum within the bracket without fail. It always moves from the current known minimum into the larger segment of the bracketed interval, as shown in Figure 1.7. The distance moved from the current position is always a fraction equal to  $\frac{3-\sqrt{5}}{2}$ , which is known as the golden section. It can be shown that using the golden section will minimize the worst case error taking the step might cause.

On the other hand, parabolic interpolation may converge on the minimum in only a few iterations. Then again, it might flail about wildly and never converge at all. This procedure involves fitting a parabola to the bracketing interval and the current known minimum, then choosing the minimum of the parabola to be the new minimum of the function. In general, there is no reason to believe that the function can be well approximated by a parabola at all, which is why this method can fail so spectacularly. Of course, if we are sufficiently close to the minimum of the function, or if the function is sufficiently smooth, Taylor's theorem tells us that a parabola will be a good approximation. The trick is to use parabolic interpolation as long as it behaves, and switch to the golden section search otherwise. Brent's method cleverly accomplishes this task in a robust and efficient way.

When the dimensionality of the problem is greater than one, the simplex method must be used. A simplex is a geometric structure that exists in  $R$ -dimensional space with  $R+1$  vertices. In two-space it is a triangle, and in three-space it is an irregular tetrahedron. In optimization, each vertex is a point somewhere on the topology of the function. On each iteration, a new vertex is chosen for the simplex that attempts to move the structure downhill. Normally, downhill movement is accomplished by reflection,

where the highest vertex is given up for a lower one opposite it, or contraction toward the lowest vertex.

Figure 1.8 shows an example function for the current problem. The details of how it was generated and the relevant constraints are discussed in Chapter 2. Suffice to say that it represents a two-dimensional optimization problem, and the third dimension in the figure is present simply to emphasize the topology of the function. The simplex is a triangle in the two-dimensional space, and each iteration will (hopefully) move the triangle closer to the floor of the valley. Note that the simplex algorithm assumes infinite space, so I had to impose the problem's constraints artificially. The function is undefined outside of the boundary formed by the line with x- and y-intercept equal to 0.5, as well as anywhere outside of the first quadrant. The steep cliff at the boundary is the result. I decreased the height of the cliff for easier visualization. More discussion about the difficulties caused by artificially imposing the constraints can be found in Chapter 2.

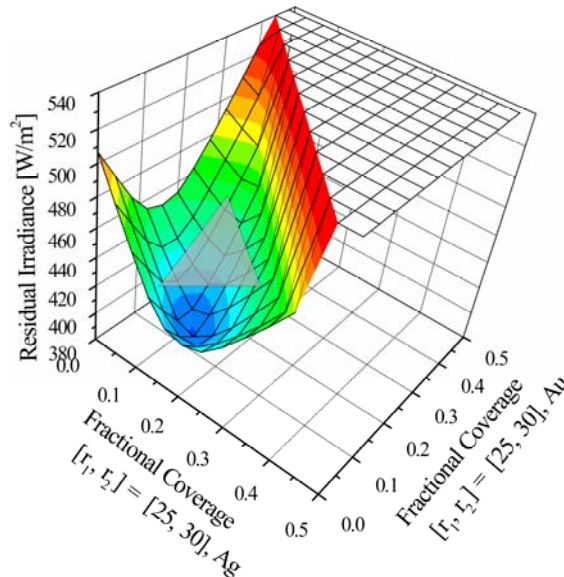


Figure 1.8 Graphical representation of a simplex on the function to be minimized. On each iteration, a new vertex will be chosen for the simplex that attempts to move it toward the valley floor.

From this introduction, it is easy to see how nanoshells can be tuned over the optical spectrum for use in solar applications. However, it is not clear which nanoshells would be best, or in what proportion to mix them. In the following chapters I expand on how I used the optimization algorithms described above to find answers to these questions.

## **Chapter 2 - Description of the Algorithm**

The goal of this project is to calculate the optimal mixture of different nanoshell species (core and shell sizes) to absorb or scatter solar energy. I accomplish this goal by using Mie theory coupled with standard optimization algorithms as implemented in Matlab. I also give a brief overview of effective techniques for using my code to solve such problems and discuss implicit approximations required to make this problem tractable.

### **Overview of the Code**

The Matlab code, as listed in Appendix A, is liberally commented, so I will only describe it here briefly. The flow is as follows:

- 1) assign values for constants and parameters,
- 2) open and read data files that contain particle cross sections,
- 3) calculate the mixture that maximizes absorbed or scattered light for each unique combination of particle species,
- 4) track the combination of species that gives optimal results, and
- 5) report the answer.

The user defines the desired core sizes, shell thicknesses, shell material (silver or gold), and dielectric embedding medium to be included in the optimization. Filenames for Mie calculations are assembled from this information in a standard format, but can be easily changed to suit the individual needs and preferences of the user.

My algorithm searches the path specified by the variable 'shell\_path' for the required data files. If any data is missing, the program creates a file named 'required\_runs.out' with a list of missing files and exits. Otherwise, the program

maintains the data files in memory so as to avoid time-consuming disk accesses. For a well designed run, the memory required is on the order of 1 MB.

All possible unique combinations of data are passed to the ‘find\_local\_min’ function, where the user is able to set various convergence parameters and select between Brent’s method for one-dimensional optimization or the simplex method for multi-dimensional problems. More information about the built-in Matlab functions used here and the convergence parameters that control them can be found on the Mathworks website<sup>25</sup>. Both methods are capable of solving the one-dimensional problem, and both arrive at the same solution, as expected. However, Brent’s method is simpler and faster than the simplex method.

The function ‘residual’ is minimized by one of the above methods. It calculates the amount of light not absorbed or scattered by the particles. Written mathematically, the function is

$$\int I(1 - \sum_R c_i q_i) d\lambda ,$$

where  $I$  is the solar irradiance,  $c$  is the cross sectional area physically covered by particle species  $i$ ,  $q$  is the efficiency of the particle,  $R$  is the number of particles in the mixture, and the integral is taken over wavelength. For each combination of species, this equation is minimized using the  $c_i$ ’s as the optimization parameters. The user specifies the total coverage of the particles on the surface as a constant ( $\sum_R c_i = c_{total}$ ), so there are  $R-1$  dimensions or degrees of freedom in the problem. The function checks that the total absorption or scattering cross sections for all the particles on the surface is less than unity ( $1 - \sum_R c_i q_i > 0$ ) to ensure that a unit area of the surface does not absorb or scatter more

light than is incident upon it. If the inequality is false for a given wavelength, the absorbed or scattered light is capped by whatever is available in the AM 1.5 spectrum.

From a general viewpoint, the code is useful in any situation that requires finding an optimal mixture of component curves to approximate a target curve. For example, this work focuses exclusively on optimally converting solar energy into other forms, so the ASTM AM 1.5 standard solar spectrum<sup>21</sup> is loaded as a target curve. Any target curve whatsoever would be equally acceptable. Additionally, all of the particle cross sections, which are the component curves, are calculated externally and supplied as data files. This arrangement allows maximum flexibility in adapting the code to future applications. For instance, one possibility is the calculation of optimal mixtures of asymmetrical nanoshells to fit an experimental nanoshell spectrum as an alternative to the much debated mean free path dielectric function modification<sup>26, 27</sup>.

### **Use of the Code**

Given that there are  $\frac{N!}{(N-R)!R!}$  unique combinations of particle species, where  $N$

is the number of different species, some finesse is recommended in selecting species for trial so that  $N$  is minimized. Judicious choice of particle geometry can dramatically help the situation. Generally speaking, large particles tend to scatter and small particles tend to absorb. Therefore, it makes sense to limit overall particle size to the most logical regime for the problem at hand. A guideline might be that absorption problems will require particles smaller than 150 nm, and scattering problems require particles larger than 100 nm. Additionally, the spectral peak position is partially controlled by shell

thickness, so it makes sense to maximize the range of that parameter using the fewest core and shell sizes.

Another technique is to start with sparse size increments and hone in on the correct result in future runs. For example, if I want to find the best single particle for absorbing sunlight with a surface coverage of 23%, I might start by choosing four cores sizes (0, 50, 100, and 150 nm) and six shell thicknesses (5, 10, 15, 20, 25, and 30 nm). If I consider both gold and silver shells, there are 48 unique combinations. Finding that the best answer is  $[r_1, r_2] = [50, 60]$  nm, I might try core sizes in 5 nm increments from 25 nm to 75 nm and shell thicknesses in 1 nm increments from 7 to 13 nm. After checking a total of only 202 unique combinations, I will find the best answer to be  $[r_1, r_2] = [40, 51]$  nm. This is almost an eighth the number of checks necessary to search the whole space in 5 nm core size increments and 1 nm shell size increments.

It is important to note that the technique may settle on a local minimum, completely missing a sharp global minimum lurking between the core and shell sizes included in the original run. If the spacing between shell thicknesses is small enough, that outcome will usually be avoided; sparsely spaced cores tend to be acceptable. From an engineering standpoint, the computational time saved must be weighed against the possibility of missing the optimal solution.

After selecting the shell species to run, it is important to consider the total surface coverage expected for the system. Surface coverage is a major constraint that can drastically change the optimization results. Figure 2.1 shows how the minimization function, and therefore the optimal mixture ratio for given nanoshell species, changes as total surface coverage is increased for a representative example. There is no guarantee

species chosen for a particular coverage will continue to be the best choice if coverage is increased. Without a specific scenario in mind, I can only outline general guidance about what to choose for this parameter.

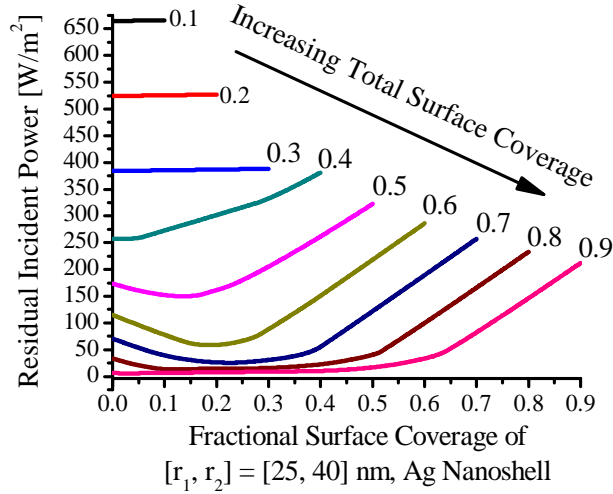


Figure 2.1 Variation of minimization function for mixture of silver shells with  $[r_1, r_2] = [25, 40]$  nm and gold shells with  $[r_1, r_2] = [55, 65]$  nm as coverage is increased

Experimentally, we regularly find interparticle spacing of about one particle diameter when we deposit nanoshells on a surface. An upper limit of surface coverage in this regime is easily found by calculating coverage for a hexagonal array of nanoparticles with spacing of one diameter. The result is coverage of approximately 23%, as shown in Appendix B. We also have the ability to create close-packed arrays of particles that cover up to 62% of the surface<sup>28</sup>. Note that high surface coverage can reduce the accuracy of the result because of particle coupling issues as discussed below.

Finally, consider the choice of convergence parameters used in the ‘find\_local\_min’ function. Brent’s algorithm tends to converge regularly regardless of the parameters chosen, but the simplex method can be more finicky. Part of the problem

is the sudden change in the residual at the boundary of the region where the function to be minimized is defined. Brent's method poses no problem because the minimum is bracketed ahead of time, but the simplex method only recognizes an infinitely continuous space. That means that it will try solutions that are not allowed by the surface coverage constraints. For example, if the total surface coverage is specified to be  $c_{total} = 0.3$ , it may try a solution with  $c_1 = 0.4$  and  $c_2 = -0.1$ . The code prevents unphysical results by automatically setting the residual to the maximum value (no light is absorbed or scattered) when the optimization values fall outside the permissible domain.

When the minimum is located on this boundary, the simplex method does not converge quickly. It is possible to solve this problem by increasing the maximum allowable number of iterations and function evaluations, but unbearably long execution times will result. A better solution is to increase the termination tolerance, 'TolX,' which controls the accuracy the computer requires for a solution. Usually, convergence continues until the answer is within the square root of the floating point accuracy of the machine, as that value is the best the computer can accomplish<sup>29</sup>. In this case, we are optimizing for mixtures of nanoshells with poorly known concentration in solution, so it makes no sense to find optimal surface coverage to eight decimal places. That precision would be impossible to reproduce when making real samples in the laboratory.

### **Inherent Approximations**

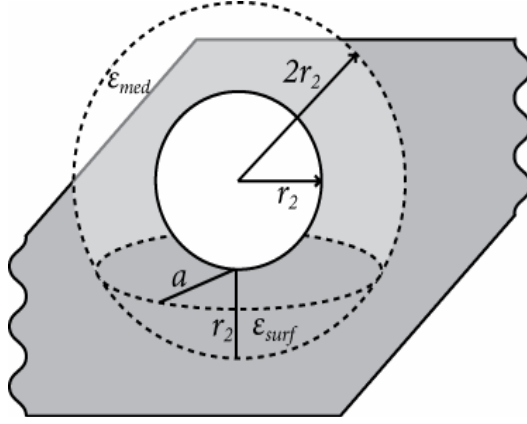
As stated previously, particle cross sections for each shell species are calculated externally and supplied as data files. I employed Mie scattering theory to calculate the particle's absorption and scattering efficiencies as a function of wavelength. This theory

does an excellent job of predicting the scattering and absorption cross sections of dilute nanoshell suspensions in a homogenous medium<sup>30</sup>. Unfortunately, there are several confounding factors that make it difficult to naively apply Mie theory to the current optimization problem.

First is the fact that many energy conversion problems, particularly the conversion of electromagnetic to electrical energy, require the plasmonic particles to be deposited on a surface. Naturally, the homogeneity of the environment is destroyed by the presence of the surface. The asymmetry of the surrounding medium causes an increase in the net dipole moment of higher order plasmon resonance modes, which allows light to couple with those modes more efficiently. This effect is particularly strong for the component of the incident electric field oriented perpendicular to the surface<sup>31</sup>. As a result, Mie theory may underestimate the strength of the quadrupole mode relative to the dipole in a complicated way that depends on the incidence angle and polarization of the light. Furthermore, the resonance energy will shift because of hybridization with surface plasmon states if the surface has free electrons in its conduction band<sup>32</sup>.

A crude, but useful, approximation of these effects is to assume a homogenous effective medium<sup>6</sup> for the particle environment by calculating a weighted average of the surface and medium dielectric functions ( $\epsilon_{eff}(\omega) = w_1\epsilon_{surf}(\omega) + w_2\epsilon_{med}$ ). Appropriate weights can be determined geometrically if the particle's optical properties are affected only by the dielectric environment within one particle radius<sup>33</sup>. The weights would then be equal to the ratio of the volume of surface to the total volume within that distance and the volume of medium to the total. Figure 2.2 shows the geometry involved. Although this solution is less than ideal because it cannot accurately model the affect of the surface

on relative peak height and shape, it does partially correct for changes in peak position. This design tradeoff enables quick calculation of absorption and scattering efficiencies for extremely large numbers of particles with standard Mie theory, at the expense of modeling the quadrupole peak well.



The volume of the surface that is within 1 radius of the particle is

$$V = \frac{1}{3} \pi r_2^2 (6r_2 - r_2) = \frac{5}{3} \pi r_2^3$$

Therefore,

$$w_1 = \frac{\frac{5}{3} \pi r_2^3}{\frac{4}{3} \pi (8r_2^3 - r_2^3)} = \frac{5}{28}$$

and

$$w_2 = 1 - w_1 = \frac{23}{28}.$$

Figure 2.2 Dielectric environment of a nanoshell on a surface – the environment within 1 particle radius contributes to the optical response

The second problem is the close proximity of particles on the surface. The particles cannot necessarily be treated as independent. It is clear from conservation of energy that when two particles are close enough for their extinction cross sections to overlap, light incident on the overlapping area is not extinguished by both particles. That is, it cannot be absorbed twice. Therefore, the total extinction cross section of the two is not simply the sum of the independent cross sections. Hybridization between the particles via columbic forces can change the scattering profile so completely that it is insufficient to correct the cross section by subtracting the overlap area from the total<sup>34</sup>. Furthermore, conducting substrates can enhance coupling between particles<sup>35, 36</sup>.

In order to gain some insight about the magnitude of the error introduced by plasmonic coupling, I investigated these effects for a specific example using the T-matrix method with code that is freely available from NASA<sup>37</sup>. Figure 2.3 shows the probability

light will scatter from a dimer system as a function of interparticle spacing. The distance dependence is oscillatory so that sometimes the probability is enhanced and sometimes it is diminished. In a worst case scenario, assuming independent particles will result in a misestimate of the scattering probability by 4%.

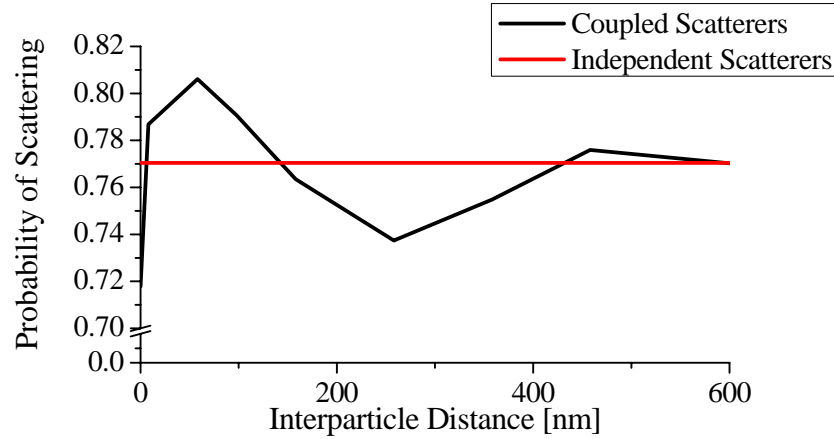


Figure 2.3 Comparison of the probability a gold colloid dimer will scatter light with 558 nm wavelength if the particles are treated as independent scatterers versus if they are treated as a coupled two particle system; the particles have radii equal to 82 nm and 60 nm

To estimate the number of particles that will be affected by coupling, consider that interparticle spacing will be governed by Poisson statistics, as shown in Appendix C. Therefore, the most probable number of particle couplings in a unit area is

$$\frac{1}{2} \pi x^2 d^2,$$

where  $x$  is the concentration of particles on the surface and  $d$  is a parameter that defines the interparticle spacing at the limit of the validity of independent scattering. The difficulty of this problem lies in the determination of the parameter  $d$  and the efficient calculation of dimer cross sections for the statistical distribution of interparticle distances less than  $d$ . Spacing greater than two particle diameters is a rough estimate of the distance required for interparticle coupling effects to be negligible<sup>38</sup>. The best way to

reduce the error introduced is to keep the nanoparticle surface coverage low, although results are still meaningful for higher coverage if one is mindful of the approximations involved.

The last complicating factor is multiple scattering effects. This factor refers to the possibility that light scattered by one particle is subsequently absorbed by another.

Fortunately, consideration of the angular dependence of the differential scattering cross section reveals that scattering occurs predominately in the forward and backward directions, as shown in Figure 2.4. Since the particles that might subsequently absorb scattered light lie at right angles to the direction of incidence, I expect multiple scattering to be a negligible effect. Furthermore, the effect will be an issue only for large nanoshells because smaller particles tend to scatter less.

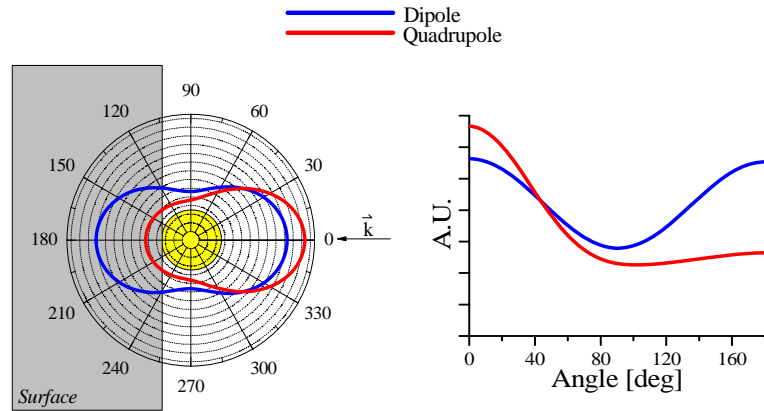


Figure 2.4 Angular dependence of scattering for unpolarized light incident normal to the surface with wavelength equal to the dipole resonance and the quadrupole resonance; a homogenous effective medium is assumed

The algorithm described here uses various approximations that are necessary to make computation time realistic. While accuracy suffers slightly as a result, the solution

still contains considerable information. The quadrupole mode in particular will be susceptible to error because of these approximations. However, it is unlikely that an ideally optimal solution will differ significantly from the reported results.

## **Chapter 3 - Two Scenarios in Detail**

I used my optimization algorithm to solve two scenarios of practical interest. The first scenario is using plasmonic particles to couple sunlight into a silicon photodiode, and the second is to maximize visible light scattering from a glass surface. These are two of many interesting applications and are only meant to serve as an example of the possibilities.

### **Absorption of Sunlight on a Silicon Photodiode**

In 2005, Schaadt et al.<sup>3</sup> demonstrated that gold colloid deposited on a silicon p/n junction can enhance the photocurrent by 80% with surface coverage as low as 1%. The mechanism for this effect is not well understood, but it is clear from unpublished experiments that it only occurs for absorptive particles. If colloid can couple light into the junction so dramatically, it should be possible to take advantage of the tunability of nanoshells to maximize the absorption of the incident light and fully exploit the enhancement.

My algorithm searched for the best mixture of nanoshells for absorbing AM 1.5 sunlight with wavelengths between 300 and 1100 nm. Wavelengths longer than 1100 nm have energy less than the band gap of silicon and will not participate in the generation of photocurrent. Both gold and silver particles were allowed. I used Johnson and Christy's<sup>39</sup> data for the dielectric function of gold, the CRC Handbook of Chemistry and Physics<sup>40</sup> for silver, and the Handbook of Optical Constants of Solids<sup>41</sup> for silicon. Since

small plasmonic particles tend to be the best absorbers, I focused on  $r_1 < 85$  nm, and surface coverage was capped at 40%.

The optimal result is a mixture of only two species, both gold nanoshells, that absorbs  $582 \text{ W/m}^2$  out of  $805 \text{ W/m}^2$  available. The first species is  $[r_1, r_2] = [47, 58]$  nm with coverage of 27.8%, and the other is  $[r_1, r_2] = [28, 42]$  nm with coverage of 12.2%. Correcting for particle size, it will require six of the larger species for every five of the smaller to achieve the desired coverage ratio. Mixing the species in this 6:5 ratio will enable absorption of nearly three-quarters of the incident irradiation as shown in Figure 3.1. Allowing mixtures of three or more species does not increase the absorbed energy unless surface coverage is also allowed to increase. If total surface coverage is increased to 50%, an additional  $96 \text{ W/m}^2$  can be harvested from the light as shown in Figure 3.2. On a real surface, interparticle effects would enable the particles to absorb the low energy light that is considered “residual” by my algorithm.

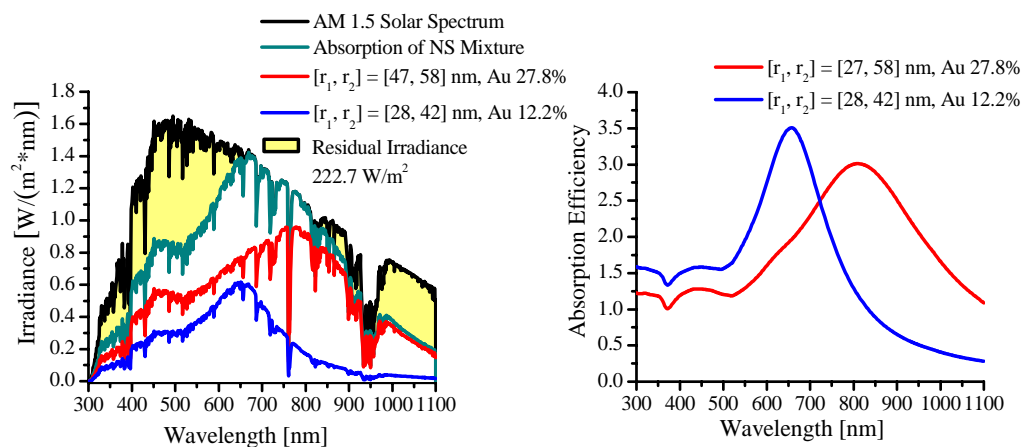


Figure 3.1 Optimal spectra of light absorbed for a silicon surface 40% covered by particles

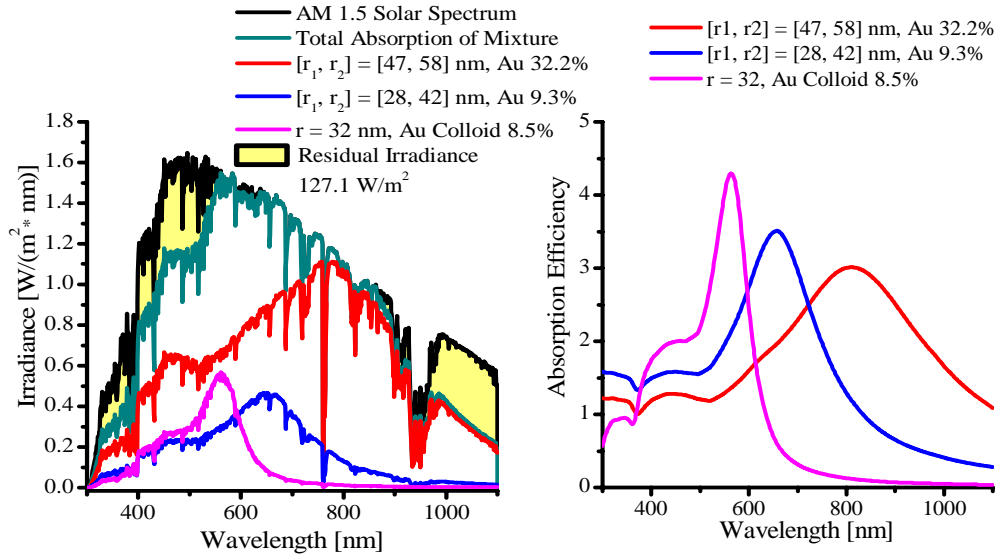


Figure 3.2 Optimal spectra of light absorbed for a silicon surface 50% covered by particles

It is interesting to consider how these “black” surfaces compare to a surface painted black with some traditional surface coating. Obviously, black paint is nearly a perfect absorber of light in the visible wavelength region. In order to keep the comparison fair, I will consider a submonolayer of paint particles with total surface coverage equal to 40%. Black pigment is almost always made from carbon<sup>42</sup>, and Mie scattering theory was successfully used to describe clusters of soot by many researchers<sup>43</sup>. I will model black paint as small (20 nm) spherical particles and use the complex index of refraction of soot (1.75+i0.435) reported by d’Almeida et al.<sup>44</sup>. Surely, this leap can be no worse than modeling the radar cross section of sparrows using bird-sized balls of water<sup>45</sup>.

Figure 3.3 shows the absorption efficiency of carbon soot from 300 to 1100 nm. The optical behavior is relatively flat across the wavelength region of interest with a

distinct lack of resonance behavior. The black color of soot originates from this even and smooth absorption spectrum. However, the optical efficiency is extremely low. As a result, at 40% surface coverage, the particles only absorb a miniscule 48 W out of 805 W available in a square meter of sunlight. Some studies show that absorption cross sections of soot aggregates are vastly enhanced by interparticle effects<sup>43</sup>, and in absolute terms, thick coats of black paint have absorptivity greater than 90%<sup>46</sup>. But, in terms of absorbing solar energy with sparse surface coverage, black paint simply cannot compete with plasmonic particles.

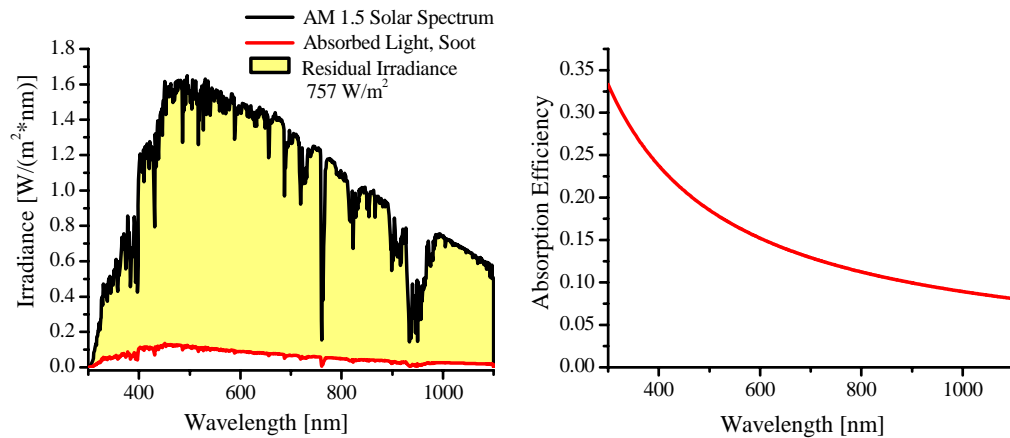


Figure 3.3 Absorption spectrum of soot

### Scattering of Sunlight from a Glass Surface

The second scenario I will discuss is optimizing light scattering from a glass surface. This problem is interesting in that it is the inverse of the absorption problem, and because it may find useful application in window treatments or other surface modifiers. The Romans used the attractive optical scattering properties of gold and silver

colloid in the 4th century for coloring glass. One of the most famous examples is the Lycurgus Cup, on display at the British Museum. The cup normally appears green, but changes color to red if viewed with a light source in transmission.

In this example, I optimize for wavelengths limited to the visible, between 380 and 820 nm. I took the dielectric constant of glass to be 2.04 over the entire domain of wavelengths. As before, both gold and silver particles are allowed, and their complex index of refraction was taken from the same sources used previously. I expected large particles to be the optimal scatterers, so I concentrated on nanoshells with cores larger than 160 nm diameter, and large colloid.

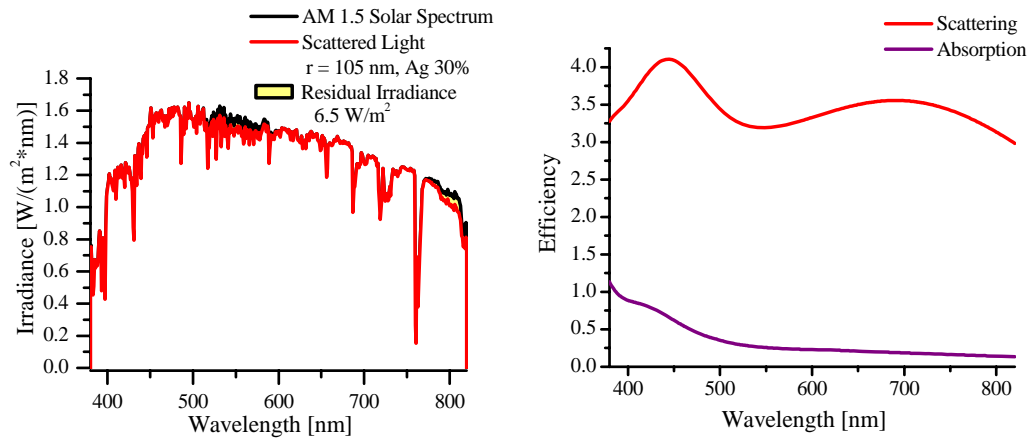


Figure 3.4 Optimal spectra of light scattered for a glass surface 30% covered by particles

Initially, I permitted total surface coverage to be 40%, but it turns out that coverage of 30% is sufficient to scatter almost all of the incident irradiation:  $571.5 \text{ W/m}^2$  out of  $578 \text{ W/m}^2$ . I was further surprised to find that a single particle species is all that is required to achieve this feat. The best particle for the job is silver colloid with a diameter

of 210 nm. Its scattering efficiency and spectrum under AM 1.5 irradiation is shown in Figure 3.4.

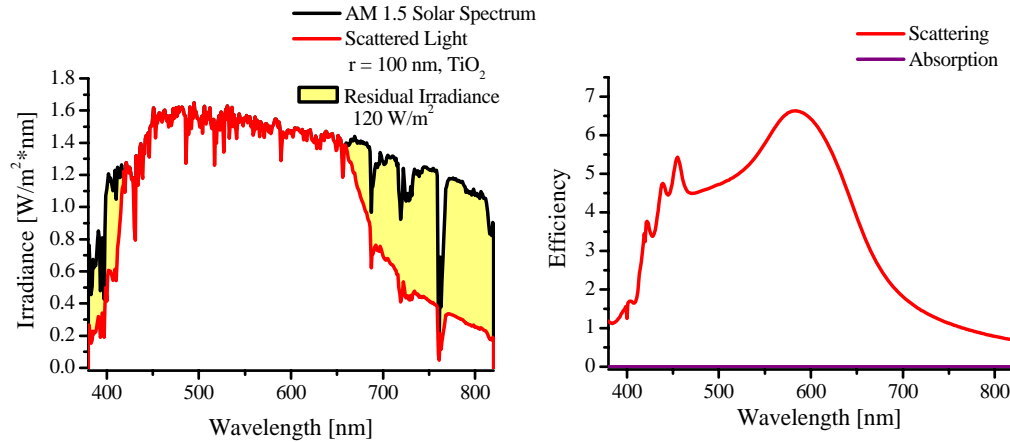


Figure 3.5 Scattering spectrum of TiO<sub>2</sub>

To gain some insight about how the performance of this particle compares to the visible light scattering of everyday objects, I show the scattering spectrum of the main ingredient of white paint. White pigment can be made from a variety of oxides, but one of the best is titanium dioxide<sup>42</sup>. Unlike carbon, titanium dioxide has very high extinction efficiency with pronounced peaks, as shown in Figure 3.5. I used the index of refraction listed in the Handbook of Optical Constants of Solids<sup>47</sup>. Titanium dioxide does not scatter the low energy light well, and with 30% surface coverage it only scatters 458 W/m<sup>2</sup>. However, TiO<sub>2</sub> will still appear to be more brilliantly white than silver colloid because its absorption spectrum is nearly zero for all visible wavelengths. Silver colloid absorbs blue light, making it look reddish-brown. The fact that TiO<sub>2</sub> does not scatter red light well may leave it with a blue tinge, but silver will still be less white. The

code does not correct for the absorption spectrum when optimizing for scattering. Including interparticle effects would eliminate the difficulties caused by that omission.

In summary, both example scenarios show that plasmonic nanoparticles are excellent tools for designing optical behavior. They can be used in both absorption and scattering applications for converting solar energy into other usable forms. Gold nanoshell species  $[r_1, r_2] = [47, 58]$  nm mixed with  $[r_1, r_2] = [28, 42]$  nm is optimal for absorbing sunlight, and silver colloid with  $r = 105$  nm is best for scattering. The particles' naturally broad ensemble resonances are ideal for interacting with broadband sunlight. Using this optimization code allows researchers to quickly determine the best particle for a given experiment, and hopefully it will enable informed design choices for nanotechnological optical devices of the future.

## **Chapter 4 – Conclusions and Future Work**

Physical understanding of how nanoshells interact with their environment could be used to improve the algorithm as it now stands. Some examples of the physical processes involved are discussed in Chapter 2. Future improvements to the code should incorporate those effects. Additionally, an engineering improvement that could decrease computation dramatically would be to use an optimization algorithm to search all realistic nanoshell species. It is subtle, but there are actually two optimization problems being solved. The first is optimizing the mixture ratio given a set of nanoshell species. The second is to optimize the set of species. In the current algorithm, brute force is used to determine the optimal group of nanoshell species. If an optimization algorithm were substituted for this brute force method, the computational time saved could be applied to more comprehensive calculations of interparticle effects.

In this work, I demonstrated how well-known optimization algorithms can be applied to solve an engineering problem in one nanoscale system – harnessing sunlight using mixtures of nanoshells on a surface. As we learn more about how to predict and control the unique properties of nanoshells, applying engineering techniques to realize novel devices becomes important. The code written for this project should be useful for a wide range of problems as we attempt to find new ways to use nanoshells in devices. Developing nanoshell applications, and more generally advancing the field of nanotechnology, are truly multi-disciplinary endeavors: chemistry controls the properties of nanoscale matter, physics is used to understand them, and engineering exploits them.

## Appendix A - Code

```

solarfit.m
1 num_species = 4;           %Number of different shell species in mix
2 lambda = [300:1700 1702 1705:5:1800].'; %Wavelengths, col vector only
3 cores = [0 25:10:55];      %core radii to try
4 shells = [5:5:25 75];      %shell thicknesses to try
5 metal_types = ['Ag','Au'];  %shell metal types to try
6 terms = 3;                 %maximum l quantum number to use
7 coverage = 0.4;            %fractional unit area covered by shells
8 interaction = 'absb';       %use 'scat' or 'absb'
9 medium = 'Glass';          %embedding medium tag
10
11 [m_rows,m_cols] = size(metal_types);
12 num_cores = length(cores);  %get number of cores
13 num_shells = length(shells); %get number of shells
14 species = m_rows.*num_cores.*num_shells; %# of species to try
15 combinations = prod([species- ... %N!/((N-R)!R!) possible combos
16     num_species+1:species])./(factorial(num_species));
17
18 runs_needed = 0;
19 shell_path = ...           %path to Mie calculation data
20 '/home/joecole/solar_spectrum_fitting/aashell_data/broad/';
21
22 load_spec_aml_5;           %load the solar spectrum
23 I_total = sum(I_tilt);      %integrate solar spec over wavelength
24
25 open_shell_files;          %load all Mie data into memory
26
27 fprintf(1,'Checking %d combinations of %d:\n', ...
28     combinations,num_species);
29
30 ind2 = [];
31 count = 0;
32 resid_light_min = I_total;  %initialize to max possible value
33 for ind = [1:combinations]  %try every combination
34     if(mod(ind,200)==0)      %give user screen output
35         fprintf(1, '.')      %so they know something's happening
36         count = count + 1;
37         if(count==70), fprintf(1,'\n'), count=0; end
38     end
39
40     ind2 = next_combo(species,num_species,ind2);
41     %get indices for Mie data to use in this iteration
42     [ad2,resid_light(ind)] = ...
43         find_local_min(I_tilt,coverage,C_eff(:,ind2));
44     %find optimal coverage ratio for this mixture
45
46     if(resid_light(ind) <= resid_light_min)
47         %if this is the best mix so far ...
48         resid_light_min = resid_light(ind); %save the answer
49         ad2_min = ad2; %save the optimization parameters
50         ind_min = ind2; %save the indices
51     end

```

```

52 end    %next iteration...
53
54 fprintf(1,'Done.\n')
55
56 fprintf(1,'\nBest answer is:\n')    %write the best answer to screen
57 for m=[1:num_species]
58     [i,j,k] = ind2sub([m_rows,num_cores,num_shells],ind_min(m));
59     fprintf(1,'\tR1 = %3d, R2 = %3d, Shell Type = %s, Coverage =
60     %5.2f%%\n',
61     cores(j),shells(k)+cores(j),metal_types(i,:),coverage.*100);
62 end

```

### **find local min.m**

```
1 function [d,y] = find_local_min(I,coverage,eff)
2 %function [d,y,err] = find_local_min(I,coverage,eff)
3 %finds the optimal density for mixtures of shell species on a
4 %surface
5 %I - column vector with elements representing the irradiance at
6 %   each wavelength
7 %coverage - scalar representing fraction of unit area physically
8 %covered by shells
9 %   (pi/(8*sqrt(3)) is good)
10 %eff - matrix of effective cross sections (num of wavelengths rows
11 %and number
12 %   of shell species columns
13
14 [wavelen,numspec] = size(eff);      %get # of wavelengths and R
15 frac_cov = ones(1,numspec-1).*coverage./numspec;
16     %initialize with equal coverage for all species
17
18 options = optimset('Display','Notify','TolX', ...
19     1e-4,'MaxFunEvals',6000,'MaxIter',4000);
20     %Set the convergence parameters
21 %[d,y,err] = fminbnd(@(x) sum(residual(x,coverage,I,eff)), ...
22 %   0,coverage,options);
23 %   Brent's method; uncomment for 1-d
24
25 [d,y,err] = fminsearch(@(x) sum(residual(x,coverage,I,eff)), ...
26     frac_cov,options);
27 %   Simplex method; uncomment for multi-d
```

### **residual.m**

```
1 function y = residual(frac_coverage,coverage,I,eff)
2 %function y = residual(frac_coverage,coverage,I,eff)
3 %finds the optimal density ratio for species of shells on a surface
4 %frac_coverage - Each column is the fraction of a unit area
5 physically covered by
6 %     that shell species. This is a row vector with one fewer
7 columns
8 %     than the number of columns in eff or extinct.
9 %I - column vector with elements representing the irradiance at
10 %    each wavelength
11 %coverage - scalar representing fraction of unit area covered by
12 shells
13 %eff - matrix of effective scattering or absorption cross sections
14 %     (num of wavelengths rows and number of shell species columns)
15 %The output is a column vector of the residual light for each
16 wavelength
17
18 resid = 1;
19 [wavelens,num] = size(eff);
20 frac_coverage(num) = coverage - sum(frac_coverage);
21     %calculate coverage for last species using constraint equation
22
23 if((frac_coverage>=0) & (frac_coverage<=coverage))
24 %if the optimization parameter for each species is in the allowed
25 %domain
26     frac_cov = ones(wavelens,1)*frac_coverage; %expand to allow
27                                           %multiply
28     resid = 1-sum(frac_cov.*eff,2); %multiply and sum on per
29                                           %wavelength basis
30     ind = find(resid < 0); %look for unphysical results
31     resid(ind) = 0; %fix unphysical results
32 end
33
34 y = I.*resid; %multiply by solar spectrum
```

### **next\_combo.m**

```
1 function [combo] = next_combo(N, R, current_combo)
2 %function [combo] = next_combo(N, R, current_combo)
3 %Calculates the indices of the next set of species
4 %N - number of different species (total)
5 %R - number of species in a set
6 %current_combo - indices of current set of species
7
8 if(~isempty(current_combo)) %if already initialized...
9     if(R ~= length(current_combo)) %if programming error...
10         disp('Argument current_combo too long in next_combo()');
11         disp('<CTRL> - C to quit');
12         combo = zeros(1,R);
13         pause
14     end
15
16     for i = [1:R]
17         if((current_combo(i) < i) | (current_combo(i) > N-R+i))
18             %if programming error...
19             disp('Argument current_combo out-of-range in ...
20             next_combo()');
21             disp('<CTRL> - C to quit');
22             combo = zeros(1,R);
23             pause
24         end
25     end
26
27     combo = current_combo;
28     combo(R) = combo(R) + 1; %counts to next index
29
30     for i = [R:-1:2] %if overflow then carry the one...
31         if(combo(i) > (N-R+i))
32             combo(i-1) = combo(i-1) + 1;
33             for j = [i:R]
34                 combo(j) = combo(j-1) + 1;
35             end
36         end
37     end
38
39     if(combo(1) > (N-R+1)) %if programming error ...
40         disp('Function next_combo() called too many times. ');
41         disp('<CTRL> - C to quit');
42         combo = zeros(1,R);
43         pause
44     end
45 else %if not already initialized...
46     combo = [1:R]; %initialize for 1st time through loop
47 end
```

### **load spec am1 5.m**

```
1 load 'ASTMG173.csv' -ascii      %load standard am 1.5 spectra
2 lambda_indexes = pick_lambdas(ASTMG173(:,1),lambda);
3     %choose wavelengths
4 Etr = ASTMG173(lambda_indexes,2);
5     %Extraterrestrial irradiance (AM0)
6 I_tilt = ASTMG173(lambda_indexes,3);
7     %Irradiance for tilted plane
8 %I_direct = ASTMG173_2(lambda_indexes,4);
9     %Direct irradiance
10
11 clear ASTMG173 lambda_indexes;      %clear unneeded variables
```

### **load\_shell\_data.m**

```
1 function [xsec] = load_shell_data(filename, lambdas, xsec_type)
2 %function xsec = load_shell_data(filename, lambdas, xsec_type)
3 %   opens a shell *.ext file and returns the effective absorption or
4 %   scattering cross section for the shell
5 %filename - full path to needed file
6 %lambdas - wavelengths needed for run
7 %xsec_type - type of interaction (absorption or scattering) to solve
8 %           for
9
10 if(nargin==2)      %figure out which column is needed
11     xsec_type = 'absb';
12 end
13
14 if(xsec_type == 'scat')
15     ind = 2;
16 elseif(xsec_type == 'absb')
17     ind = 3;
18 elseif(xsec_type == 'extn')
19     ind = 4;
20 else
21     disp('I do not understand the third argument you provided to
22 load_shell_data().');
23     disp('<CTRL> - C to quit');
24     pause
25 end
26
27 shell_data = load(filename, '-ascii');
28     %load the required data
29 lambda_indexes = pick_lambdas(shell_data, lambdas);
30     %select required wavelengths
31 xsec = shell_data(lambda_indexes, ind);
32     %select required column
```

### **pick\_lambdas.m**

```
1 function inds = pick_lambdas(data,lambda)
2 %function inds = pick_lambdas(data,lambda)
3 %checks data to make sure the wavelengths needed for the run exist
4 %and selects the indices of those wavelengths
5 %these must be in increasing order, because the function only
6 %searches the portion of data that hasn't been checked before in
7 %order to shorten the run time
8 %
9 %data - vector of wavelengths present in the data
10 %lambda - vector of wavelengths needed for run
11
12 i = 1;
13 e = length(data);
14 inds = [];
15
16 for l = lambda.'
17     ind = find(l == data(i:e)) + i - 1;
18     % find next required wavelen
19     if(length(ind) ~= 1)
20         disp('Unable to find specified lambda in function
21 pick_lambdas()');
22         disp('<CTRL>-C to quit');
23         pause
24     end
25     i = ind+1;
26     inds = [inds;ind];          %append new index to end of list
27 end
```

## Appendix B- Surface Coverage Calculation

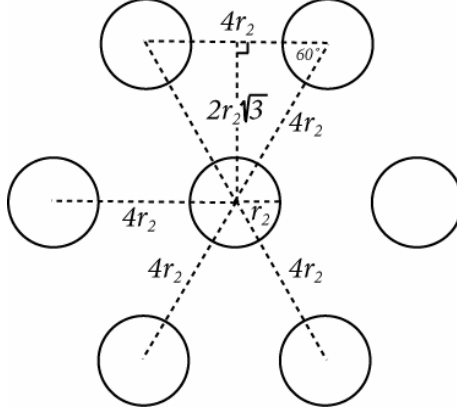


Figure B.1 Hexagonal array of nanoparticles with one diameter spacing between them.

The surface can be divided into 30-60-90 triangles with a base  
and height

$$b = 2r_2,$$

$$h = 2\sqrt{3}r_2.$$

The area of the circle inside the triangle is

$$\frac{1}{4}\pi r_2^2,$$

therefore, the surface coverage is:

$$\frac{\frac{1}{4}\pi r_2^2}{\frac{1}{2}bh} =$$

$$\frac{\pi r_2^2}{8\sqrt{3}r_2^2} =$$

$$\frac{\pi}{8\sqrt{3}} \approx 0.23.$$

## Appendix C-

### Number of Interparticle Couplings on a Surface

Imagine a surface with area  $A$ . Particles are added at random to the surface one-by-one. When the  $N$ th particle is added, it causes  $N-1$  Bernoulli trials. We define *success* to mean that the particle lands within a distance  $d$  of another particle, close enough for interparticle coupling effects to be relevant. The probability of success is

$$p = \frac{\pi d^2}{A}.$$

The probability of failure is

$$q = 1 - \frac{\pi d^2}{A}.$$

As  $N$  increases, the number of trials per unit area is

$$\frac{n}{A} = \frac{1}{A} \sum_{i=1}^N i = \frac{N^2 + N}{2A} \approx \frac{N^2}{2A}$$

for large  $N$ . Since  $n/A$  tends toward infinity as  $O(N^2)$ , Poisson's approximation will give good estimates for this binomial distribution. The mean of Poisson's distribution (per unit area) is known to be

$$\lambda = \frac{np}{A} \approx \frac{N^2 \pi d^2}{2A^2},$$

which also equals its standard distribution. The concentration of particles per unit area,  $x$ , can be written as

$$x = \frac{N}{A},$$

leaving us with the most probable number of interparticle couplings per unit area:

$$\lambda = \frac{1}{2} \pi x^2 d^2.$$

Note that this is *not* the number of coupled particles because each particle can be coupled with multiple others. This estimate includes all the couplings. We can find a lower bound on the number of coupled particles by noting that there are

$$\frac{k!}{(k-2)!2!}$$

possible two-particle couplings for  $k$  particles. Solving for  $k$ , we arrive at the quadratic equation:

$$\begin{aligned} \frac{k(k-1)}{2} &= \frac{1}{2} \pi x^2 d^2 \\ k^2 - k - \pi x^2 d^2 &= 0 \\ \frac{1 \pm \sqrt{1 + 4\pi x^2 d^2}}{2} &= k \end{aligned}$$

## References

- 1) McFarland, E. W., and J. Tang. "A Photovoltaic Device Structure Based on Internal Electron Emission." Nature 421.6923 (2003): 616-618.
- 2) Gratzel, M. "Photoelectrochemical Cells." Nature 414 (2001): 338-344.
- 3) Schaadt, D. M., B. Feng, and E. T. Yu. "Enhanced Semiconductor Optical Absorption Via Surface Plasmon Excitation in Metal Nanoparticles." Applied Physics Letters 86.6 (2005): 063106.
- 4) Polarization is technically related to the difference between the electric field,  $\vec{E}$ , and the electric displacement,  $\vec{D}$ , whereas the dielectric function is related to their ratio. However, introduction of the electric susceptibility,  $\chi$ , shows the equivalence of the two. See reference 8 for more information.
- 5) Ashcroft, N.W., and N.D. Mermin. Solid State Physics. College ed. Fort Worth: Harcourt College Publishers, 1976.
- 6) Kreibig, U., and M. Vollmer. Optical Properties of Metal Clusters. Springer Series in Materials Science. Eds. U. Gonser, et al. Berlin: Springer-Verlag, 1995.
- 7) Powell, C. J., and J. B. Swan. "Origin of the Characteristic Electron Energy Losses in Aluminum." Physical Review 1.4 (1959): 869-875.
- 8) Born, M., and E. Wolf. Principles of Optics. 7 ed. Cambridge: Cambridge University Press, 2002.
- 9) Raether, H. Surface Plasmons on Smooth and Rough Surfaces and on Gratings. Berlin: Springer-Verlag, 1988.
- 10) Sokolov, K., et al. "Real-Time Vital Optical Imaging of Precancer Using Anti-Epidermal Growth Factor Receptor Antibodies Conjugated to Gold Nanoparticles." Cancer Research 63 (2003): 1999-2004.
- 11) Haes, A. J., and R. P. Van Duyne. "A Nanoscale Optical Biosensor: Sensitivity and Selectivity of an Approach Based on the Localized Surface Plasmon Resonance Spectroscopy of Triangular Silver Nanoparticles." Journal Of The American Chemical Society 124.35 (2002): 10596-10604.
- 12) Pillai, S., et al. "Enhanced Emission from Si-Based Light-Emitting Diodes Using Surface Plasmons." Applied Physics Letters 88 (2006): 161102.
- 13) Mie, G. "Beitrage Zur Optik Trueber Medien Speziell Kolloidaler Metalloesungen." Annalen Der Physik 25 (1908): 377-445.

- 14) Aden, A.L., and M. Kerker. "Scattering of Electromagnetic Waves from Two Concentric Spheres." Journal of Applied Physics 22 (1951): 1242-1246.
- 15) Prodan, E., et al. "A Hybridization Model for the Plasmon Response of Complex Nanostructures." Science 302 (2003): 419-422.
- 16) Oldenburg, S. J., et al. "Nanoengineering of Optical Resonances." Chemical Physics Letters 288.2-4 (1998): 243-247.
- 17) Bohren, C.F. "How Can a Particle Absorb More Than the Light Incident on It?" American Journal of Physics 51.4 (1983): 323-327.
- 18) Wang, Z.B., et al. "Energy Flow around a Small Particle Investigated by Classical Mie Theory." Physical Review B 70 (2004): 035418.
- 19) "Sun." The New Encyclopedia Britannica, 11 (1990): 387-388.
- 20) Rybicki, G.B., and A.P. Lightman. Radiative Processes in Astrophysics. New York: John Wiley & Sons, Inc., 1979.
- 21) American Society for Testing and Materials Standard ASTM G-173-103. "Standard Tables for Reference Solar Spectral Irradiance at Air Mass 1.5: Direct Normal and Hemispherical for a 37 Degree Tilted Surface". 2003. National Renewable Energy Laboratory. Accessed: 18 April 2006.  
<<http://rredc.nrel.gov/solar/spectra/am1.5/>>.
- 22) This entire section is written following the excellent treatment given in reference 29. I strongly encourage interested readers to start there in pursuit of further information.
- 23) Brent, R.P. Algorithms for Minimization without Derivatives. Englewood Cliffs, NJ: Prentice-Hall, 1973.
- 24) Nelder, J.A., and R. Mead. Computer Journal 7 (1965): 308-313.
- 25) 2006. MathWorks. Accessed: 18 April 2006.  
<<http://www.mathworks.com/access/helpdesk/help/helpdesk.html>>.
- 26) Nehl, C.L., et al. "Scattering Spectra of Single Gold Nanoshells." Nano Letters 4.12 (2004): 2355-2359.
- 27) Berciaud, S., et al. "Observation of Intrinsic Size Effects in the Optical Response of Individual Gold Nanoparticles." Nano Letters 5.3 (2005): 515-518.

- 28) Wang, H., C. S. Levin, and N. J. Halas. "Nanosphere Arrays with Controlled Sub-10-Nm Gaps as Surface-Enhanced Raman Spectroscopy Substrates." Journal Of The American Chemical Society 127.43 (2005): 14992-14993.
- 29) Press, W.H., et al. Numerical Recipes in C, the Art of Scientific Computing. Cambridge: Cambridge University Press, 1992.
- 30) Averitt, R. D., D. Sarkar, and N. J. Halas. "Plasmon Resonance Shifts of Au-Coated Au<sub>2</sub>S Nanoshells: Insight into Multicomponent Nanoparticle Growth." Physical Review Letters 78.22 (1997): 4217-4220.
- 31) Gozhenko, V.V., and L.G. Grechko. "Electrodynamics of Spatial Clusters of Spheres: Substrate Effects." Physical Review B 68 (2003): 125422.
- 32) Le, F., et al. "Plasmons in the Metallic Nanoparticle-Film System as a Tunable Impurity Problem." Nano Letters 5.10 (2005): 2009-2013.
- 33) Evanoff, D.D., Jr., R.L. White, and G. Chumanov. "Measuring the Distance Dependence of the Local Electromagnetic Field from Silver Nanoparticles." Journal of Physical Chemistry B 108 (2004): 1522-1524.
- 34) Nordlander, P., et al. "Plasmon Hybridization in Nanoparticle Dimers." Nano Letters 4.5 (2004): 899-903.
- 35) Felidj, N., J. Aubard, and G. Levi. "Enhanced Substrate-Induced Coupling in Two-Dimensional Gold Nanoparticle Arrays." Physical Review B 66 (2002): 245407.
- 36) Stuart, H.R., and D.G. Hall. "Enhanced Dipole-Dipole Interaction between Elementary Radiators near a Surface." Physical Review Letters 80.25 (1998): 5663-5666.
- 37) Mishchenko, M.I. 2006. Accessed: 18 April 2006.  
<[http://www.giss.nasa.gov/~crmim/t\\_matrix.html](http://www.giss.nasa.gov/~crmim/t_matrix.html)>.
- 38) Mishchenko, M.I., L.D. Travis, and A.A. Lacis. Scattering, Absorption, and Emission of Light by Small Particles. 2nd Electronic ed. Cambridge: Cambridge University Press, 2002.
- 39) Johnson, P. B., and R. W. Christy. "Optical-Constants of Noble-Metals." Physical Review B 6.12 (1972): 4370-4379.
- 40) Lide, D.R. CRC Handbook of Chemistry and Physics. 81 ed: CRC Press, 2000.
- 41) Ribarsky, M.W. Handbook of Optical Constants of Solids. Academic Press Handbook Series. Ed. E.D. Palik. 1 ed. Washington, D.C.: Academic Press, Inc., 1985.

- 42) "Chemical Process Industries: Paints and Varnishes." The New Encyclopedia Britannica, 21 (1990): 317-322.
- 43) Liu, L., and M. I. Mishchenko. "Effects of Aggregation on Scattering and Radiative Properties of Soot Aerosols." Journal Of Geophysical Research-Atmospheres 110 (2005): D11211.
- 44) d'Almeida, G.A., P. Koepke, and E.P. Shettle. Atmospheric Aerosols: Global Climatology and Radiative Characteristics. Hampton, VA: Deepak, 1991.
- 45) Bohren, C.F., and D.R. Huffman. Absorption and Scattering of Light by Small Particles. New York: John Wiley & Sons, Inc., 1983.
- 46) Moore, J.H., C.C. Davis, and M.A. Coplan. Building Scientific Apparatus: A Practical Guide to Design and Construction. 3 ed. Cambridge, MA: Perseus Books, 2003.
- 47) Edwards, D.F. Handbook of Optical Constants of Solids. Ed. E.D. Palik. 1 ed. Washington, D.C.: Academic Press, Inc., 1985.